SPECTROSCOPIC STUDY OF IRAS 19285+0517(PDS 100): A RAPIDLY ROTATING Li-RICH K GIANT

Bacham E. Reddy and David L. Lambert

Department of Astronomy, University of Texas, Austin, TX 78712;

ereddy@astro.as.utexas.edu, dll@astro.as.utexas.edu

Bruce J. Hrivnak[1]

Department of Physics and Astronomy, Valparaiso University, Valparaiso, IN 46383;

bruce.hrivnak@valpo.edu

Eric J. Bakker

Leiden Observatory, P.O. Box 96864, 9513, 2300 RA Leiden, The Netherlands;

bakker@strw.leidenuniv.nl

Received ________________; accepted ________________

[1]Visiting astronomer, Kitt Peak National Observatory. KPNO is operated by the Association of Universities for Research in Astronomy, Inc. under contract with the National Science Foundation.

ABSTRACT

We report on photometry and high-resolution spectroscopy for IRAS 19285+0517. The spectral energy distribution based on visible and near-IR photometry and far-IR fluxes shows that the star is surrounded by dust at a temperature of $T_{\rm d} \sim 250$ K. Spectral line analysis shows that the star is a K giant with a projected rotational velocity $v\,sini = 9 \pm 2$ km s^{-1}. We determined the atmospheric parameters: $T_{\rm eff} = 4500$ K, log $g = 2.5$, $\xi_t = 1.5$ km s^{-1}, and [Fe/H] = 0.14 dex. The LTE abundance analysis shows that the star is Li-rich (log ϵ(Li) = 2.5±0.15), but with essentially normal C, N, and O, and metal abundances. Spectral synthesis of molecular CN lines yields the carbon isotopic ratio ^{12}C/^{13}C = 9 ±3, a signature of post-main sequence evolution and dredge-up on the RGB. Analysis of the Li resonance line at 6707 Å for different ratios ^{6}Li/^{7}Li shows that the Li profile can be fitted best with a predicted profile for pure ^{7}Li. Far-IR excess, large Li abundance, and rapid rotation suggest that a planet has been swallowed or, perhaps, that an instability in the RGB outer layers triggered a sudden enrichment of Li and caused mass-loss.

Subject headings: stars: abundances-stars:individual (IRAS19285+0517)-stars: K giant

1. INTRODUCTION

Observations of lithium in the atmospheres of red giants continue to pose theoretical challenges. Stars evolving up the red giant branch from the main sequence develop a deep convective envelope that dilutes the surface lithium abundance. Thus, red giants are predicted to have a lithium abundance considerably below the initial or interstellar

abundance of log ϵ(Li)≈3.0. Classical calculations (Iben 1967) predict a reduction by a factor of 30 and 60 for solar metallicity stars of 1 $M_{\odot}$ and 3 $M_{\odot}$, respectively. If some lithium has been destroyed prior to evolution off the main sequence, the red giant's lithium abundance will be even further reduced. However, as a very luminous asymptotic red giant (4-7 M$\odot$), theory and observations show that surface lithium can be replenished and even increased above the initial or interstellar abundance thanks to hot bottom burning in intermediate-mass stars (Sackmann & Boothroyd 1992).

This paper is concerned with a red giant that has yet to evolve to the asymptotic giant branch but that has a lithium abundance greatly in excess of that expected of a star on the red giant branch. Wallerstein & Sneden (1982) discovered the first such red giant: HD 112127 with $\log \epsilon(\mathrm{Li}) \simeq 3.0$, i.e., the interstellar value. In the last two decades, additional examples have been discovered; Charbonnel & Balachandran (2000) list 17 stars (including 3 subgiants, 2 early-AGB stars, and 2 for which evolutionary status has yet to be determined) with $\log \epsilon(\mathrm{Li}) \geq 2.0$, and include several additional examples with a lower lithium abundance which is most probably in excess of that expected of a red giant. Three of the 17 stars have a lithium abundance clearly greater than the stars' probable initial value. Charbonnel & Balachandran (2000) lists $v\,sini$ values for 22 giants of which 10 have $v\,sini > 8$ km s^{-1}. If we include the PDS 365 (Drake et al. 2001) and the IRAS 19285+0517 (present study), the number of Li-rich giants for which $v\,sini > 8$ km s^{-1} rises to 12. It now appears that more than half of the Li-rich giants are rotating at a unusually high rate for normal K giants for which average $v\,sini \sim 2.0$ (de Medeiros et al. 2000). This proportion drops to a mere 2% for the more common slowly rotating K giants (Drake et al. 2001). Most of them exhibit a pronounced infrared excess (Gregorio-Hetem et al. 1992; Gregorio-Hetem, Castilho, & Barbuy 1993).

Here, we report an analysis of a K giant with large infrared excess, first reported to be

a Li-rich candidate by de la Reza et al. (1997). The star is IRAS 19285+0517, also known as PDS100 after the Pico dos Dias Survey (de la Reza, Drake, & da Silva 1996). No prior quantitative spectroscopy of this star has been reported. We show from high-resolution echelle spectra that the star is Li-rich ($\log \epsilon(\mathrm{Li}) \simeq 2.5$) and rapidly rotating ($v\, sini \simeq 9$ km s^{-1}).

2. OBSERVATIONS

2.1. Photometry

Standardized photometry was carried out for this object at the Kitt Peak National Observatory (KPNO). Visible photometry was made using a CCD on the 0.9 m telescope on 1995 September 13 and near-infrared observations were made using the Cryogenic Optical Bench (COB) infrared camera on the 2.1 m telescope on 1995 October 12. The results are listed in Table 1.

The object is red, with B−V = 1.48. Some of the reddening may be due to interstellar extinction and some also due to circumstellar extinction. An effective reddening of $E(B-V) = (B-V)_{obs} - (B-V)_{pred} = 0.34$ was estimated using a predicted color B-V = 1.14 for the derived atmospheric model (next section) and synthetic colors computed by Girardi et al. (2000). The visible photometry is corrected for extinction using the extinction curve computed by Seaton (1979), and the near-infrared values are corrected for extinction using the relationship between infrared and visible extinction (Cardelli, Clayton, & Mathis 1989). Flux-converted photometry is compared with the Kurucz (http://cfaku5.harvard.edu) flux model for $T_{\rm eff} = 4500$ K, log $g = 2.5$, [Fe/H] = 0.0 in Figure 1. IRAS infrared fluxes at 12 μm, 25 μm, and 60 μm are well above the expected fluxes, indicating an infrared excess. A black body fit to the IRAS fluxes indicates a

dust temperature (T_d) of about 250 K. In sharp contrast, the IRAS fluxes of the K giant Arcturus are well fit by the predicted photospheric fluxes (see Figure 1).

2.2. High-Resolution Spectroscopy

A high-resolution spectrum of IRAS 19825+0517 was obtained on 1997 October 17 with the McDonald Observatory's 2.7 m telescope using the cross-dispersed echelle spectrograph (Tull et al. 1995). Three spectra were recorded on a CCD, each with an exposure of 20 minutes. A Th-Ar hollow cathode lamp was observed between the stellar exposures. The spectra were reduced in the standard fashion using the IRAF[2]. The final combined spectrum has a signal-to-noise ratio S/N $\simeq$ 350 in the continuum at 6500 Å and a resolving power of $\lambda/\Delta\lambda \simeq 55,000$, as measured from the comparison lines. The usable spectrum covers the wavelength interval from about 5000 Å to 9500 Å with gaps between echelle orders longward of 5680 Å. Below 5000 Å the lines are too blended and the S/N ratio is too low for analysis.

Inspection of the spectrum confirmed the great strength of the Li I 6707 Å line, the atypical widths of all absorption lines, and unusual profiles of the Na D and Hα lines (Figure 2). Both Hα and Na D profiles are seen to be asymmetric. An asymmetric Hα profile is common in Li-rich K giants (Drake et al. 2001) and is attributed to chromospheric activity in the star. The core (deepest part of the line) of the Hα profile is at the systemic velocity (V$_r$) of 2.0$\pm$1.5 km s^{-1}. The Na D profiles are complex. The line cores are asymmetric like Hα. There is a strong absorption at -16 km s^{-1} with respect to the

---

[2]IRAF is distributed by the national Optical Astronomical Observatories, which is operated by the Association for Universities for Research in Astronomy, Inc., under contract to the National Science Foundation.

systemic velocity. This may be due to circumstellar gas but we can not exclude the possibility of an interstellar origin. More interesting is the shallow broad blue-shifted absorption. This component is surely of circumstellar origin.

3. ANALYSIS

For the abundance analysis we adopted the widely used grid of LTE model atmospheres computed by Kurucz (http://cfaku5.harvard.edu). The models are available in steps of 250 K ($T_{\rm eff}$), 0.5 dex (log g), and 0.5 dex ([M/H]). Required models were interpolated. Another basic requirement in the abundance analysis is a set of reliable gf-values for the selected lines. For many of the transitions, laboratory measured gf-values are available. For the rest of the transitions we chose reliable theoretical values. For iron, a large number of Fe I and Fe II line gf-values were reviewed by Lambert et al. (1996). For other elements, we used the large compilation of R.E. Luck (1993, private communication). All of the atomic data were examined by deriving abundances for the Sun and the K giant Arcturus. Equivalent widths (W_λ) for the Sun were measured using the spectrum of the asteroid Iris (reflected solar spectrum) obtained with the same instrument as that used for our program star. In the case of Arcturus, we used high-resolution digitized spectra published by Hinkle et al. (2000).

3.1. Atmospheric Parameters

Effective temperature ($T_{\rm eff}$), surface gravity (log g), microturbulent velocity (ξ_t), and chemical composition (in short, [Fe/H]) are essential atmospheric parameters. For IRAS 19285+0517, the atmospheric parameters are determined spectroscopically. Standard procedures are not directly applicable here because the high rotational velocity increases

the blending of lines and reduces the number of useful lines. In a modification of the standard procedure, we first determined ξ_t and then proceed to the determination of the latter parameters.

To determine ξ_t we chose combination of weak and strong lines of the same species and with similar lower excitation potentials (LEP). Differences in abundance from the strong and weak line (DABUN(s-w)) were computed for a range of ξ_t. Line combinations from Fe I, Co I, and Ni I were considered; details are given in Table 2. The condition DABUN(s-w) = 0 provides ξ_t. Figure 3 shows the run of DABUN(s-w) vs ξ_t for the selected pairs. All intersect DABUN(s-w) = 0 at a similar value of ξ_t; we adopt $\xi_t = 1.5 \pm 0.1$ km s^{-1}. This result is insensitive to the adopted $T_{\rm eff}$ and $\log g$. We found the $T_{\rm eff}$ insensitivity for pairs of Fe I, Co I, and Ni I lines by computing DABUN(s-w) for four different values of ξ_t for models spanning 600 K in $T_{\rm eff}$.

Having determined ξ_t, we found $T_{\rm eff}$ in the usual way by demanding that a model atmosphere return the same Fe (Ni) abundance from a large number of Fe I (Ni I) lines with a range in LEP. The 38 Fe I lines used range in LEP from 0.96 eV to 5.0 eV and the 32 Ni I lines range from 1.6 eV to 4.4 eV. Surface gravity has little effect on the $T_{\rm eff}$ determination. Both sets of lines yield $T_{\rm eff} = 4500 \pm 100$ K.

Application of ionization balance using the previously determined ξ_t and $T_{\rm eff}$ then gives an estimate of the surface gravity with the abundance of the metal used in the exercise. Neutral and singly-ionized lines of Fe, Cr, and Ti give three independent estimates of $\log g$. The number of lines in each solution is (n_{atom}, n_{ion}) = (32,8), (8,2), and (9,4), and these lead to $\log g$ solutions of 2.7, 2.3, and 2.5 for Fe, Cr, and Ti, respectively. We adopt a mean value $\log g = 2.5 \pm 0.25$. The iron abundance (relative to the Sun) determined is [Fe/H] = +0.14±0.16.

As a check on our choice of lines and atomic data, we derived atmospheric parameters

for Arcturus, a slowly rotating bright K giant of similar $T_{\rm eff}$ and log g but of lower [Fe/H]. For our selection of lines, we measured equivalent widths (W_λ) from the high-resolution spectral atlas published by Hinkle et al. (2000). A determination of ξ_t from the pairs of Fe I and Ni I lines gave $\xi_t = 1.6 \pm 0.3$ km s^{-1}. The Fe I lines of different LEP required a model with $T_{\rm eff} = 4275 \pm 50$ K. Ionization balance applied to Fe I and Fe II lines gave $\log g = 1.5 \pm 0.25$ with [Fe/H] = -0.58 ± 0.1. The results from these selected lines are in excellent agreement with the results of Peterson et al. (1993) from a very detailed analysis, namely $T_{\rm eff} = 4300 \pm 30$ K, $\log g = 1.5 \pm 0.15$, $\xi_{\rm t} = 1.7$ km s^{-1}, and [Fe/H] = -0.50 ± 0.1. The derived atmospheric values are given in Table 3.

3.2. Physical Parameters: $v\,sini$, V$_r$, and L

The projected rotational velocity of IRAS 19285+0517 was estimated by fitting a synthetic spectrum to the portions of the observed spectrum. In addition to microturbulence, collisional broadening, and rotation, we included macroturbulence. This was modeled as a Gaussian distribution function with parameter V_m for which we adopted $V_m = 3$ km s^{-1}, a value typical of K giants (Fekel 1997). Using the current version of the spectrum synthesis code MOOG (Sneden 1973), we synthesized profiles of a few strong lines. The standard form of rotational broadening was assumed (Gray 1992) with a limb-darkening coefficient ϵ taken from Wade & Rucinski (1985). Figure 4 shows fits to Fe I and Ni I lines at 6173.3 Å and 6175.3 Å, respectively. Observed profiles are fitted by varying only $v\,sini$ and keeping macroturbulence, instrumental profile width (FWHM = 0.15 Å), and abundances constant. Note that the predicted profile for the $v\,sini = 2.0$ km s^{-1} for normal K giants (De Medeiros et al. 2000) is far too sharp to match the observed profile. A profile for $v\,sini = 9 \pm 2$ km s^{-1} best fits the observed profiles. The result is insensitive to the adopted value of $V_{\rm m}$; if the macroturbulence is neglected, $v\,sini = 9.5$ km s^{-1} is found.

Another important quantity is the heliocentric radial velocity $V_{\rm r}$ = 2.0± 1.5 km s^{-1} (Observing date: 1997 October 17 and 01:37:22 UT), derived using the wavelength shifts of many symmetric absorption features. The measurements of V$_r$ for lines of LEP in the range of 0 - 9 eV show that the measured $V_{\rm r}$ is independent of LEP.

The evolutionary status of IRAS 19285+0517 may be assessed from its luminosity, which we determine from the standard expression derived from the relations $L \propto R^2 T_{\rm eff}^4$ and $g \propto M/R^2$:

$$\log \frac{L}{L_\odot} = \log \frac{M}{M_\odot} - \log g + 4 \log T_{\rm eff} - 10.61 \qquad (1)$$

Given the derived $T_{\rm eff}$ and $\log g$, we obtain $\log L/L_\odot = 1.5 \pm 0.2$ for an assumed mass of $1M_\odot$ and $\log L/L_\odot$ = 1.8 for $2M_\odot$. As judged by its location in the H-R diagram, IRAS 19285+0517 is probably a He-core burning or clump giant. Evolutionary tracks computed by Bertelli et al. (1994) for the composition Z = 0.02 and Y = 0.28 put the clump giants at log L/L$_\odot$ = 1.7 and $T_{\rm eff}$ = 4500 K after 10^{10} yrs for a mass M ≈ 1 M$_\odot$ at the main sequence turn-off.

4. CHEMICAL COMPOSITION

A thorough abundance analysis was made using a Kurucz convective model atmosphere having the adopted atmospheric parameters. For selected elements, spectrum synthesis was conducted but for most elements unblended lines could be found. We discuss the results under the headings: general metal abundance, lithium, and C, N, and O abundances.

4.1. General Metal Abundances

Lines of elements from Al to Nd were identified despite the moderate rotational line broadening. Identifications were checked against the high quality spectrum of Arcturus (Hinkle et al. 2000). The entire line list was checked against equivalent widths measured from the spectrum of the asteroid Iris, and where necessary gf-values were adjusted. Table 4 summarizes the abundances $\log \epsilon(\mathrm{X})$ and the abundance ratios relative to solar abundances [X/H] and [X/Fe]. Solar abundances ($\log\ \epsilon(\mathrm{X})_{\odot}$), except for C, N, and O, are adopted from Grevesse & Sauval (1998). For C, N, and O we adopted the abundances derived in this study using the solar spectrum. Uncertainties in the derived abundances are given in the form of σ_{tot}, where σ_{tot} is the quadratic sum of various sources of uncertainties: the gf-values, the measured W_{λ} (represented by line-to-line scatter), and the derived atmospheric parameters (Table 3) . During the abundance analysis we estimated the uncertainties in the model parameters: $\delta T_{\mathrm{eff}} = 100$ K, $\delta\log\ g = 0.25$, and $\delta\xi_{\mathrm{t}} = 0.25$ km s^{-1}.

To within the errors of measurement, abundances from Al to Nd are normal for a star that is slightly metal-enriched relative to the Sun, i.e., [X/Fe] $\simeq 0.0$ is expected. Specifically, the s-process elements are not enriched, confirming that the star is neither a resident of the AGB nor has received mass from a companion that had evolved to the AGB.

4.2. Lithium Abundance

Initial inspection of the spectrum confirmed de la Reza et al.'s (1997) identification of IRAS 19285+0517 as Li-rich. The Li I 6707 Å resonance doublet is very strong with an equivalent width $W_{\lambda} \simeq 372$ mÅ. Owing to the blending of fine, hyperfine, and possibly isotopic components, the doublet must be analysed using spectrum synthesis. The wavelengths and line strengths of these components are taken from Smith, Lambert, &

Nissen (1998), as corrected by Hobbs, Thorburn, & Rebull (1999).

To complete the spectrum synthesis, a line list for several Ångströms around 6707 Å was compiled, primarily from Kurucz (http://cfaku5.harvard.edu). We required that this list reproduce the spectra of the Sun and Arcturus, both Li-poor objects. Then synthetic spectra for IRAS 19285+0517 were computed and broadened with the instrumental profile, the adopted macroturbulence, and rotational broadening. A good fit to the Li I line was obtained with the abundance $\log \epsilon(\mathrm{Li}) = 2.5 \pm 0.1$ (Figure 5, top panel) and the assumption that ^{6}Li is absent (see below). At this Li abundance, the excited Li I line at 6104 Å is also expected to be present. Our synthesis of this weak line (Figure 5, bottom panel) confirms the abundance derived from the resonance doublet. At $\log \epsilon(\mathrm{Li}) \simeq 2.5$, IRAS 19285+0517 certainly enters the small but growing ranks of Li-rich red giants; the Li abundance is about 1 dex greater than the maximum value expected of a red giant with a deep convective envelope.

The assumption that all lithium is ^{7}Li deserves scrutiny. Addition of ^{6}Li to the composition increases the red asymmetry of the line and shifts it to longer wavelengths (Figure 6). Synthetic profiles for different ^{6}Li/^{7}Li ratios by varying total lithium abundance were computed such that the W_λ of the predicted profile matches with that of the observed profile ($W_\lambda = 370 \pm 3$mÅ). The predicted profiles of equal W_λ, but for different ^{6}Li/^{7}Li ratios and Li abundances are compared with the overall shape of the observed profile (Figure 6; upper panel). (The Li profile is significantly saturated and addition of ^{6}Li components require less total Li abundance (relative to ^{7}Li only profile) to achieve the same W_λ of ^{7}Li only profile). The predicted profile of ^{6}Li/^{7}Li = 0.0 and log $\epsilon(\mathrm{Li}) = 2.5 \pm 0.1$ best fits with the observed profile, and ratios greater than about 0.03 are excluded. Fitting has been done by fixing the observed Li profile position (6708.832±0.02 Å) determined from Doppler shifts of symmetric Fe I and Ca I features for which accurate laboratory measurements are

available. Within the measurement errors observed Li profile position matches with the predicted profile position $\lambda_c = 6707.814$ Å (for ^{7}Li only). Lines with similar sensitivity as Li I 6707 Å to atmospheric structure are well reproduced by the synthetic spectra (e.g., the intercombination resonance Ca I line at 6572.8 Å of similar strength to the Li I line is reproduced (Figure 6, bottom panel)). This is evidence that unusual atmospheric effects are not seriously biassing the isotopic ratio.

Our abundance estimates assume LTE prevails. Carlsson et al. (1994) quantified non-LTE effects for Li I lines in red giants. In the case of the 6707 Å line, the correction for non-LTE effects is sensitive to the strength of the line. For a star of $\log g \simeq 2.0$ and $T_{\rm eff} \simeq 4500$ K with a 6707 Å of $W_\lambda \simeq 400$ mÅ, the non-LTE abundance is only about 0.1 dex lower than the LTE abundance. The non-LTE abundance for the 6104 Å line under the same conditions is about 0.2 dex greater than the LTE result. These adjustments are barely larger than the uncertainties of the LTE abundances arising from the errors in the adopted atmospheric parameters, especially the effective temperature.

4.3. C, N, and O Abundances

Our approach to finding the C,N, and O abundances was a differential one involving IRAS 19285+0517, the Sun, and α Ser. The K giant α Ser is a Li-poor giant with a $T_{\rm eff}$, log g and [Fe/H] very similar to that of IRAS 19285+0517. We analysed the same lines in all three objects and consider the differential abundances. In this way, the effects of several potential sources of error (e.g., the CN molecule's dissociation error) are mitigated, if not entirely eliminated.

Spectra of α Ser were obtained also with the McDonald Observatory's 2.7 m telescope and analysed using our standard procedures. Our derived fundamental parameters (Table 3)

show that, to within the errors of measurement, it is a 'carbon copy' of IRAS 19285+0517, apart from the great difference in lithium abundance and projected rotational velocity.

Three indicators of the carbon abundance were used: the [C I] 8727 Å line, the C I 5380 Å line, and a C_2 Swan system triplet at 5135 Å with lower weight given to another C_2 feature at 5141 Å. We took atomic and molecular data around the [C I] line from Gustafsson et al. (1999). For the 5380 Å line we adopted the theoretical log $gf = -1.57$ (Biémont et al. 1993). For the spectrum syntheses near 5135 Å (Fig 7), we took data for C_2 lines from Querci, Querci, & Kunde (1971), and for MgH and the atomic lines from Kurucz data base.

The derived carbon abundances are given in Table 5. For IRAS 19285+0517 relative to Sun, [C/H] is 0.10 (8727 Å), 0.19 (5380 Å) (Fig 8), and −0.10 (5135 Å), for a mean of 0.07. This results in a carbon abundance of [C/Fe] = −0.07, which is a mild carbon deficiency as compared to [C/Fe] = 0 as the initial ratio for stars of roughly solar metallicity. For α Ser, [C/H] is 0.10 (8727 Å), 0.15 (5380 Å), and −0.05 (5135 Å) for a mean of 0.07 or [C/Fe] = 0.07, a slight carbon enrichment relative to the initial carbon abundance.

The nitrogen abundance and $^{12}C/^{13}C$ ratio were obtained from the CN Red System lines at 8005 Å and the mean carbon abundance. Basic data for the CN lines were taken from de Laverny & Gustafsson (1998, also private communication) with a dissociation energy $D_0 = 7.75$ eV (Lambert 1993). For IRAS 19285+0517, [N/H] = 0.20, which, if [N/Fe] = 0 is appropriate for the unevolved progenitor, corresponds to a mild nitrogen enrichment of [N/Fe] = 0.06. The enrichment for α Ser is more substantial: [N/H] = 0.35 and [N/Fe] = 0.35. Syntheses of the 8005 Å region yields for IRAS 19285+0517 the isotopic ratio $^{12}C/^{13}C = 9 \pm 3$ from the ^{13}CN feature at 8004.7 Å (Fig 9). The error on the isotopic ratio was estimated as a quadratic sum of the various uncertainties. The uncertainty in C and N abundances of ±0.1 dex leads to uncertainty of ±2, respectively, in the $^{12}C/^{13}C$ ratio. The rms = 0.004 of the S/N at the continuum yields approximately an uncertainty of ±1 in the

carbon ratio. The quoted uncertainties in the derived model parameters have insignificant effect on the derived $^{12}C/^{13}C$ ratio. The ratio for α Ser was determined to be $^{12}C/^{13}C$ = 10±3, which is in good agreement with the ratio $^{12}C/^{13}C$ = 12±2 previously determined by Day, Lambert, & Sneden (1973)

Oxygen abundances are obtained from the [O I] 6300 Å line. Allowance was made for a blending Ni I line (Allende Prieto et al. 2001). IRAS 19285+0517 has [O/H] of 0.09, a value very close to the likely initial value. Oxygen in α Ser is apparently enhanced with [O/H] = 0.19. A summary of the derived mean C, N, and O abundances, and the ratios relative to Fe ([X/Fe]) for IRAS 19285+0517, α Ser, and Sun is given in Table 6.

5. DISCUSSION

5.1. Defining the Anomalies

According to the inferred luminosity and the derived effective temperature, IRAS 19285+0517 is probably a He-core burning (clump) giant. Since the red giant branch for H-shell burning stars at the luminosity of the clump is only slightly cooler than the clump, we cannot exclude the possibility that IRAS 19285+0517 is evolving to He-core ignition.

A normal giant, whether on the RGB prior to He-core ignition or at the clump as a He-core burning star, has a deep convective envelope that developed when the star was a subgiant. The result of convection is to dilute the surface lithium abundance by a factor of about 50 so that a normal lithium abundance does not exceed $\log \epsilon(\mathrm{Li}) = 1.2$. The convective envelope also brought to the surface material exposed mildly to the H-burning CN-cycle. This process reduces the surface ^{12}C abundance, reduces the $^{12}C/^{13}C$ ratio, increases the ^{14}N abundance, but is predicted to leave the ^{16}O abundance unaffected. Analyses of red giants confirm the sense of these changes but there is ample evidence that

observed changes, especially the $^{12}C/^{13}C$ ratio, are frequently more extreme than predicted by standard models.

Our reference giant α Ser is a typical giant with its $^{12}C/^{13}C$ ratio (12±3) less than predicted by standard models. Observations of the isotopic ratio in giants of the open cluster M 67 show that 'low' ($\leq$ 10) $^{12}C/^{13}C$ ratios are found only in giants that have evolved to or beyond the tip of the red giant branch (Gilroy & Brown 1991). If, as is possible, α Ser is a clump giant, its low isotopic ratio fits the pattern established by M 67. The same claim may be made for IRAS 19285+0517 but its status as a 'normal' giant is, of course, questionable.

α Ser was included by Lambert & Ries (1981) in their C, N, and O analyses of a sample of field K giants. The expected changes in C and N were revealed by this analysis. Relative to the mean abundances for the sample, α Ser was somewhat less depleted in C and less enriched in N with an approximately normal O abundance (Table 6). IRAS 19285+0517 is a close but not exact match to α Ser. The closeness of the match depends on whether the comparison is made using [X/H] or [X/Fe]. Using [X/H], the C and N abundances are very similar, possibly identical to within the errors of measurement; α Ser is slightly enriched in N and O, where the latter is presumably a reflection of a higher initial abundance. If [X/Fe] is the preferred indicator, IRAS 19285+0517 is underabundant in C, N, and O by -0.14, -0.29, and -0.24 dex, respectively, relative to α Ser. Judged with respect to the assumption that initial abundances would have satisfied the condition [C/Fe] = [N/Fe] = 0, IRAS 19285+0517 is possibly just deficient in carbon (-0.07 dex) and enriched in nitrogen (+0.06 dex). Given that a typical red giant displays larger abundance changes - [C/Fe] $\simeq -0.2$ and [N/Fe] $\simeq +0.4$ are typical (Lambert & Ries 1981) - there is a suspicion that Li-rich IRAS 19285+0517 has 'anomalous' carbon and nitrogen abundances.

The certain and pronounced anomalies of IRAS 19285+0517 are (i) its high lithium

abundance ($\log\epsilon(\mathrm{Li}) = 2.5$), (ii) its rapid rotation ($v \sin i = 9$ km s^{-1}), and (iii) its substantial infrared excess. In having these anomalies, IRAS 19285+0517 is similar HD 233517 (Balachandran et al. 2000), and PDS 365 (Drake et al. 2001). Drake et al. list the known K giants with $v \sin i \geq 8$ km s^{-1}. Of their 22 stars, 6 of the 14 with a measured lithium abundance are Li-rich. Among the few K giants with a pronounced infrared excess, about half are Li-rich (de la Reza et al. 1997). The impression given is that Li enrichment, rapid rotation, and infrared excess are causally related. That the correlation between the three observational attributes is not perfect may be due to different times and time scales for their appearance and/or disappearance; for example, surface lithium abundance may decay as lithium is destroyed internally at a rate different from the rate at which angular momentum is removed from the envelope.

5.2. Explaining the Anomalies

An assumption common to the proposed explanations of the Li-rich giants is that, as a subgiant, the star underwent the predicted severe dilution of its original lithium and the lithium was subsequently replenished at some point in the giant's evolution. This is a plausible scenario since several Li-rich giants, some slowly rotating and others rapidly rotating, have a lithium abundance greater than the star's presumed initial abundance. In addition, there are no known main sequence stars with a lithium abundance that, after standard dilution by the factor of about 30 to 50, would provide the high lithium abundance of the Li-rich giants. Therefore, proposed explanations envisage either lithium production by the giant or replenishment of surface lithium by capture of one or more planets. Explanations should be judged for plausibility not only for the lithium abundance but also by their ability to account for the existence of circumstellar material as revealed through the infrared excess and for the rapid rotation of many Li-rich giants.

Proposals invoking lithium production exploit the ^{3}He reservoir predicted to exist outside the He-core and, if present, the H-burning shell of the red giant. This reservoir was built up in the main sequence star outside its H-burning core in layers sufficiently hot for ^{3}He to be produced by the initial steps of the *pp*-chain but not so hot that ^{3}He was quickly destroyed. The giant's convective envelope that diluted the surface lithium also smeared the ^{3}He reservoir over the envelope. Given this supply of ^{3}He, the reactions $^3\mathrm{He}(\alpha,\gamma)^7\mathrm{Be}(e,\nu)^7\mathrm{Li}$ may convert ^{3}He to ^{7}Li. To achieve efficient lithium production, the ^{7}Be must be swept quickly to lower temperatures in order to avoid destruction of ^{7}Be and ^{7}Li by hot protons. This scenario of lithium production, which is commonly called the Cameron-Fowler (1971) mechanism, accounts for the Li-rich AGB stars which are predicted to have a deep convective envelope with a hot bottom.

The ^{3}He reservoir has been invoked by several authors (e.g., Sackmann & Boothroyd 1999) as the key to the Li-rich giants (i.e stars at luminosities too low for them to be identified as AGB giants) but, in many cases, the physical trigger for ^{7}Li production has not been identified. Palacios, Charbonnel, & Forestini (2001) have suggested that the burning of ^{7}Li created by depletion of the ^{3}He reservoir enables lithium to get to the surface. Rapid rotation is suggested as a way to generate a 'lithium flash' to enhance the mixing and surface abundance. This process is expected to occur when the red giant's H-burning shell burns through a discontinuity in mean molecular weight introduced previously by the development of the convective envelope. A majority of the Li-rich giants appear to be at the predicted luminosity (Charbonnel & Balachandran 2000), as estimated from their *Hipparcos* parallaxes. (The luminosity and $T_{\rm eff}$ are not very different from the prediction for He-core burning giants.) This interesting idea only in a more speculative fashion accounts for the infrared excess; the luminosity increase of about a factor of 2 during the brief flash (duration $\sim 10^3$ yrs) is blamed for the mass loss on the empirical evidence from much more luminous stars that mass loss increases with luminosity. The idea does explain why lithium

is pure ^{7}Li. If our suspicion is confirmed that the carbon and nitrogen abundances of IRAS 19285+0517 are less extreme than expected for a normal red giant, this would seem to present a difficulty for the Li-flash scenario; the predicted duration of the flash is too short to affect the abundances which should reflect fully the alterations induced by the convective envelope.

An alternative explanation for the main anomalies (Li enrichment, rapid rotation, and circumstellar matter) is the accretion by the red giant of material in the form of planets or a brown dwarf. This has been discussed to different degrees of detail by Alexander (1967), Siess & Livio (1999) and and Denissenkov & Weiss (2000).

Siess & Livio (1999) discuss the accretion of a planet or brown dwarf by 1 $M_{\odot}$ red giants of different luminosities. It is shown that the red giant may be spun up, eject mass, and become enriched in lithium. Considerable adjustments to the internal structure occur but the surface lithium enrichment results entirely from the lithium in the accreted material. If destruction of lithium is avoided, the maximum lithium abundance resulting from the accretion of giant planets or a brown dwarf is necessarily the interstellar value (say, $\log\epsilon(\mathrm{Li}) \simeq 3$). The lithium abundance of IRAS 19285+0517 is comfortably below this limit but several Li-rich stars (Charbonnel & Balachandran 2000; Drake et al. 2001) have lithium above this limit. In principle, higher lithium abundances are possible through the accretion of terrestrial planets (i.e., cosmic material less hydrogen, helium, and other volatiles), but this requires that the mass of the material from which the terrestrial planets were derived exceeds the mass of the red giant (Brown et al. 1989), which would seem to be a difficult condition to meet. Denissenkov & Weiss (2000) propose that accretion activates the Cameron-Fowler mechanism and thus the surface lithium abundance may exceed the initial value before destruction sets in.

In addition to accounting for the lithium, the rapid rotation, and the infrared excess,

accretion of giant planets or a brown dwarf serves to adjust the C and N abundances towards their initial values and away from the changed values induced by the convective envelope. If the lithium is added without subsequent destruction, the isotopic lithium ratio would be expected to be close to the initial value for the star and its natal cloud, which, on the basis of limited evidence from measurements of the ratio in local diffuse clouds, is likely to have been about ^{7}Li/^{6}Li = 10, a ratio clearly ruled out for IRAS 19285+0517. However, for this star, we cannot exclude the possibility that a small amount of lithium was destroyed subsequent to the accretion. Since ^{6}Li is destroyed about 70 times faster than ^{7}Li, even the loss of trace amounts of lithium ensures effectively complete destruction of ^{6}Li.

6. CONCLUDING REMARKS

With the discovery of extra solar planets in close elliptical orbits, accretion of giant planets by red giants is a virtual certainty. That this phenomenon can account for all of the known Li-rich giants is uncertain. Accretion without activation of the ^{3}He reservoir certainly cannot account for the super Li-rich stars which have more Li than the ISM value. It would be helpful to extend the detailed analyses of the Li-rich giants. Extensions should include a uniform abundance analysis for the light elements (and isotopes) C, N, and O for a sample including normal K giants, so that subtle differences between Li-rich and Li-normal giants may be distinguished. Extant analyses show that there are no large differences (Berdyugina & Savanov 1994; da Silva et al. 1995). Measurement of the beryllium abundance in Li-rich giants would be valuable. Accretion of a planet or brown dwarf restores the Be abundance. Conversion of the ^{3}He reservoir to ^{7}Li does not return the Be abundance to its pre-diluted value (Castilho et al. 1999).

Measurements of the ^{7}Li/^{6}Li ratio should be extended to other stars. Positive detection of ^{6}Li would favor the accretion scenario. In this regard, we note the recent detection of ^{6}Li

in the atmosphere of a main sequence star with a giant extra solar planet (Israelian et al. 2001) suggests that the star has accreted one or more former planets. Early accretion of this kind will not account for Li-rich giants like IRAS 19285+0517, because in evolution to the red giant phase, the convective envelope will dilute the lithium to below the observed abundance of IRAS 19285+0517.

We acknowledge the support of the National Science Foundation (Grant AST-9618414) and the Robert A. Welch Foundation of Houston, Texas (Grant F-634). BJH acknowledges support from the National Science Foundation (AST-9315107, AST-9900846). This research has made use of the Simbad database, operated at CDS, Strasbourg, France, and the NASA ADS service, USA.

REFERENCES

Allende Prieto, C., Lambert, D.L., & Asplund, M. 2001, ApJ, 556, L63

Alexander, J.B. 1967, The Observatory, 87, 238

Balachandran, S.C., Fekel, F.C., Henry, G.W., & Uitenbroek, H. 2000, ApJ, 542, 978

Berdyugina, S.V., & Savanov, L.S. 1994, AstL, 20, 755

Bertelli, G., Bressan, A., Chiosi, C., Fagotton, F., & Nasi, E. 1994, A&AS, 106, 275

Biémont, E., Hibbert, A., Godefroid, M., & Vaeck, N. 1993, ApJ, 412, 431

Brown, J.A., Sneden, C., Lambert, D.L., & Dutchover, E., Jr. 1989, ApJS, 71, 293

Carlsson, M., Rutten, R.J., Bruls, J.H.M.J., & Shchukina, N.G. 1994, A&A, 288, 860

Charbonnel, C., & Balachandran, S.C. 2000, A&A, 359, 563

Cameron, A.G.W., & Fowler, W.A. 1971, ApJ, 164, 111

Cardelli, J.A., Clayton, G.C., & Mathis, J.S. 1989, ApJ, 345, 245

Castilho, B.V., Spite, F., Barbuy, B., Spite, M., De Medeiros, J.R., & Gregorio-Hetem, J. 1999, A&A, 345, 249

da Silva, L., de la Reza, R., & Barbuy, B. 1995, ApJ, 448, L41

Day, R.W., Lambert, D.L., & Sneden, C. 1973, ApJ, 185, 213

de la Reza, R., Drake, N.A., da Silva, L., Torres, C.A.O., & Martin, E.L. 1997, ApJ, 482, L77

de la Reza, R., Drake, N.A., & da Silva, L. 1996, ApJ, 456, L115

de Laverny, P., & Gustafsson, B. 1998, A&A, 332, 661

De Medeiros, J.R., do Nascimento Jr, J.D., Sankarankutty, S., Costa, J.M., & Maia, M.R.G. 2000, A&A, 363,239

Denissenkov, P.A., & Weiss, A. 2000, A&A, 358, L49

Drake, N.A., de la Reza, R., da Silva, L., & Lambert, D.L. 2001, AJ, submitted

Fekel, F.C. 1997, PASP, 109, 514

Gilroy, K.K., & Brown, J.A. 1991, ApJ, 371, 578

Girardi, L., Bressan, A., Bertelli, G., & Chiosi, C. 2000, A&AS, 141, 371

Gray, D.F. 1992, The Observation and Analysis of Stellar Photospheres, (Cambridge: Cambridge Univ. Press)

Gregorio-Hetem, J., Castilho, B.V., & Barbuy, B. 1993, A&A, 268, L25

Gregorio-Hetem, J., Lépine, J.R.D., Quast, G.R., Torres, C.A.O., & de la Reza, R. 1992, AJ, 103, 549

Grevesse, N., & Sauval, A.J. 1998, Space Sci. Rev., 85, 161

Gustafsson, B., Karlsson, T., Olsson, T., Edvardsson, B., & Ryde, N. 1999, A&A, 342, 426

Hinkle, K., Wallace, L., Valenti, J., & Harmer, D. 2000 Visible and Near Infrared Atlas of the Arcturus Spectrum 3727 - 9300 Å (San Francisco: ASP)

Hobbs, L.M., Thorburn, J.A., & Rebull, L.M. 1999, ApJ, 523, 797

Iben, I., Jr. 1967, ApJ, 147, 624

Israelian, G., Santos, N.C., Mayor, M., & Rebolo, R. 2001, Nature, 411, 163

Lambert, D.L., 1993, in Molecules in the Stellar Environment, ed. U.G. Jorgensen (Berlin: Springer-Verlag), 1

Lambert, D.L., Heath, J.E., Lemke, M., & Drake, J.1996, ApJS, 103, 183

Lambert, D.L., & Ries, L.M. 1981, ApJ, 248, 228

Palacios, A., Charbonnel, C., & Forestini, M. 2001, A&A, 375, L9

Peterson, R.C., Dalle Ore, C.M., & Kurucz, R.L. 1993, ApJ, 404, 333

Querci, F., Querci, M., & Kunde, V.G. 1971, A&A, 15, 256

Sackmann, I.-J., & Boothroyd, A.I. 1992, ApJ, 393, L71

Sackmann, I.-J., & Boothroyd, A.I. 1999, ApJ, 510, 217

Seaton, M.J. 1979, MNRAS, 187, 73

Siess, L., & Livio, M. 1999, MNRAS, 308, 1133

Smith, V.V., Lambert, D.L., & Nissen P.E. 1998, ApJ, 506, 405

Sneden, C. 1973, Ph.D. thesis, Univ. of Texas at Austin

Tull, R.G., MacQueen, P.J., Sneden, C., & Lambert, D.L. 1995, PASP, 107, 251

Wade, R.A., & Rucinski, S. M. 1985, A&AS, 60, 471

Wallerstein, G., & Sneden, C. 1982, ApJ, 255, 577

This manuscript was prepared with the AAS LaTeX macros v5.0.

Fig. 1.— Spectral energy distributions of Arcturus (top panel) and IRAS 19285+0517 (bottom panel). The solid line in both cases is the predicted flux distribution from the Kurucz model atmosphere having the fundamental parameters described in the text and given in the figure. The infrared excess of IRAS 19285+0517 at 12, 25, 60, and 100 μm is evident and is fit with a 250 K black body curve

Fig. 2.— The spectrum of IRAS 19285+0517 around the Na D lines (top panel) and the Hα line (bottom panel). The vertical dashed lines labled as 1, 2, and 3 (top panel) indicate photospheric velocity, -16 km s^{-1}, and -38 km s^{-1}, respectively (see the text for details). The vertical dashed line (bottom panel) represents the photospheric velocity of the Hα.

Fig. 3.— Abundance difference between combinations of strong and weak lines of similar lower excitation potential from the same atom, DABUN(s-w), plotted against the assumed microturbulence. Results from lines of iron (solid lines), cobalt (dashed line), and nickel (dotted lines) are shown. A microturbulence $\xi_{\rm t} = 1.5 \pm 0.1$ km s^{-1} corresponding to DABUN(s-w) = 0 is adopted.

Fig. 4.— The spectrum of IRAS 19285+0517 from 6172 Å to 6176 Å showing strong Fe I and Ni I lines. The observed spectrum (filled circles) is shown together with three predicted line profiles computed from the adopted model atmosphere and identical assumptions but for the three different values of the projected rotational velocity: $v \sin i = 2, 9$, and 12 km s^{-1}. The velocity $v \sin i = 9$ km s^{-1} provides a good fit to the observed line profiles. See text for additional details.

Fig. 5.— Observed (filled circles) and synthetic spectra around the Li I lines at 6707 Å (top panel) and 6104 Å (bottom panel). The observed 6707 Å line is well matched by the synthetic spectrum computed for the abundance $\log \epsilon(^7{\rm Li}) = 2.50$. Three synthetic spectrum are shown for the 6104 Å line, with that for $\log \epsilon(^7{\rm Li}) = 2.5$ providing a satisfactory fit to

the observed spectrum.

Fig. 6.— Observed (filled circles) and synthetic spectra of the Li I 6707 Å resonance doublet (top panel) and the Ca I intercombination resonance line at 6572 Å (bottom panel). In the top panel, synthetic spectra are provided for the three isotopic ratios ^{6}Li/^{7}Li = 0.0, 0.05, and 0.10, with ^{6}Li/^{7}Li = 0.0 providing the best fit. The synthetic spectrum in the bottom panel shows that observed Ca I line is well matched by the synthetic line.

Fig. 7.— The spectrum of IRAS 19285+0517 around 5138 Å. Several MgH and C_2 lines are identified including the C_2 feature at 5135.6 Å, a primary indicator of the carbon abundance.

Fig. 8.— The spectrum of the Sun (top panel) and IRAS 19285+0517 (bottom panel) from 5379 Å to 5384 Å showing the C I the line at 5380 Å. The synthetic spectrum (solid line) shown for IRAS 19285+0517 is computed for the carbon abundance $\log \epsilon(\mathrm{C}) = 8.66$.

Fig. 9.— The spectrum of IRAS 19285+0517 around 8005 Å. Synthetic spectra (solid line) show the contributions of CN Red system lines with the ^{12}C and ^{14}N abundances fixed but the ^{12}C/^{13}C ratio set at 5, 10, and 15.

Table 1: Ground-Based Photometry for IRAS 19285+0517

Band	Mag.	log (F_ν)[a] ($ergs\ cm^{-2}\ s^{-1}\ Hz^{-1}$)
B	11.83±0.01	−23.52
V	10.35±0.02	−23.13
R_c	9.52±0.03	−22.97
I_c	8.78±0.03	−22.86
J	7.71±0.01	−22.72
H	6.98±0.02	−22.68
K	6.70±0.01	−22.83

[a] fluxes are corrected for a reddening of E(B-V) = 0.34.

Table 2: Lines used in Deriving ξ_t

Line (Å)	Iden.	LEP (eV)	log gf	W_λ (mÅ)
6692.265	Fe I	4.076	-2.899	21.3
6027.050	Fe I	4.076	-1.090	106.0
6699.200	Fe I	4.590	-2.191	41.0
6024.049	Fe I	4.548	-0.060	165.0
5367.470	Fe I	4.415	0.350	182.3
6704.500	Fe I	4.220	-2.660	31.0
6159.368	Fe I	4.607	-1.970	52.0
6293.923	Fe I	4.835	-1.605	50.0
6055.992	Fe I	4.733	-0.460	104.0
5987.066	Fe I	4.795	-0.426	115.0
6005.029	Co I	1.711	-3.320	30.0
6116.990	Co I	1.785	-2.490	72.0
6093.140	Co I	1.740	-2.440	77.0
7062.970	Ni I	1.951	-3.500	75.0
6914.560	Ni I	1.951	-2.070	158.0
6025.730	Ni I	4.236	-1.760	18.0
6086.290	Ni I	4.266	-0.530	85.0
6133.950	Ni I	4.088	-1.830	31.0
6176.810	Ni I	4.088	-0.530	102.0

Table 3: Derived Fundamental Properties

Star	[Fe/H]	$T_{\rm eff}$ (K)	$\log g$ (cm s^{-2})	ξ_t (km s^{-1})
IRAS 19285+0517	0.14±0.16	4500±100	2.50±0.25	1.55±0.1
Arcturus	−0.58±0.1	4275±50	1.5±0.25	1.6±0.3
	(−0.50±0.1)[a]	(4300±30)[a]	(1.5±0.15)[a]	(1.7)[a]
α Ser	0.0±0.1	4600±100	2.50±0.25	1.9±0.25

[a]from Peterson, Dalle Ore, & Kurucz 1993.

Table 4: Elemental Abundances of IRAS 19285+0517

Element	log $\epsilon(X)_\odot$[a]	n	log $\epsilon(X)$	σ_{tot}	[X/H]	[X/Fe]
Li I	1.10	2	2.50	0.20	...	...
Al I	6.47	3	6.73	0.07	0.26	0.12
Si I	7.55	14	7.83	0.08	0.28	0.14
Ca I	6.36	3	6.30	0.20	−0.08	−0.22
Ti I	5.02	9	5.08	0.21	0.06	−0.08
Ti II	...	4	5.04	0.23	0.02	−0.12
V I	4.00	10	4.35	0.20	0.35	0.21
Cr I	5.67	7	5.71	0.14	0.04	−0.10
Cr II	...	2	6.07	0.12	0.40	0.26
Fe I	7.50	40	7.65	0.16	0.15	0.01
Fe II	...	8	7.62	0.20	0.12	−0.02
Co I	4.92	9	5.28	0.17	0.36	0.22
Ni I	6.25	35	6.55	0.17	0.30	0.16
Zr I	2.60	8	2.66	0.19	0.06	−0.08
Ba II	2.13	3	2.67	0.22	0.54	0.40
La II	1.17	3	1.54	0.22	0.37	0.23
Nd II	1.50	5	1.72	0.20	0.22	0.08

[a]from Grevesse & Sauval 1998.

Table 5: C, N, and O Abundance Analysis of IRAS 19285+0517, the Sun, and α Ser

Feature	Sun log ϵ(X)	α Ser log ϵ(X)	IRAS 19285+0517 log ϵ(X)
Carbon			
C_2 5135 Å	8.60	8.55	8.50
C I 5380 Å	8.51	8.66	8.70
[C I] 8727 Å	8.50	8.60	8.60
Nitrogen			
CN (N) 8005Å	8.00	8.35	8.20
Oxygen			
[O I]6300 Å	8.75	8.94	8.84

Table 6: C, N, and O Abundance Summary of IRAS 19285+0517, the Sun, and α Ser

Star	[Fe/H]	log ϵ(C)	log ϵ(N)	log ϵ(O)	[C/Fe]	[N/Fe]	[O/Fe]	$^{12}C/^{13}C$
IRAS 19825+0517	0.14	8.60	8.20	8.84	-0.07	0.06	-0.05	9±1
α Ser	0.0	8.60	8.35	8.94	0.07	0.35	0.19	10±1
Sun	0.0	8.54	8.00	8.75	0.0	0.0	0.0	90

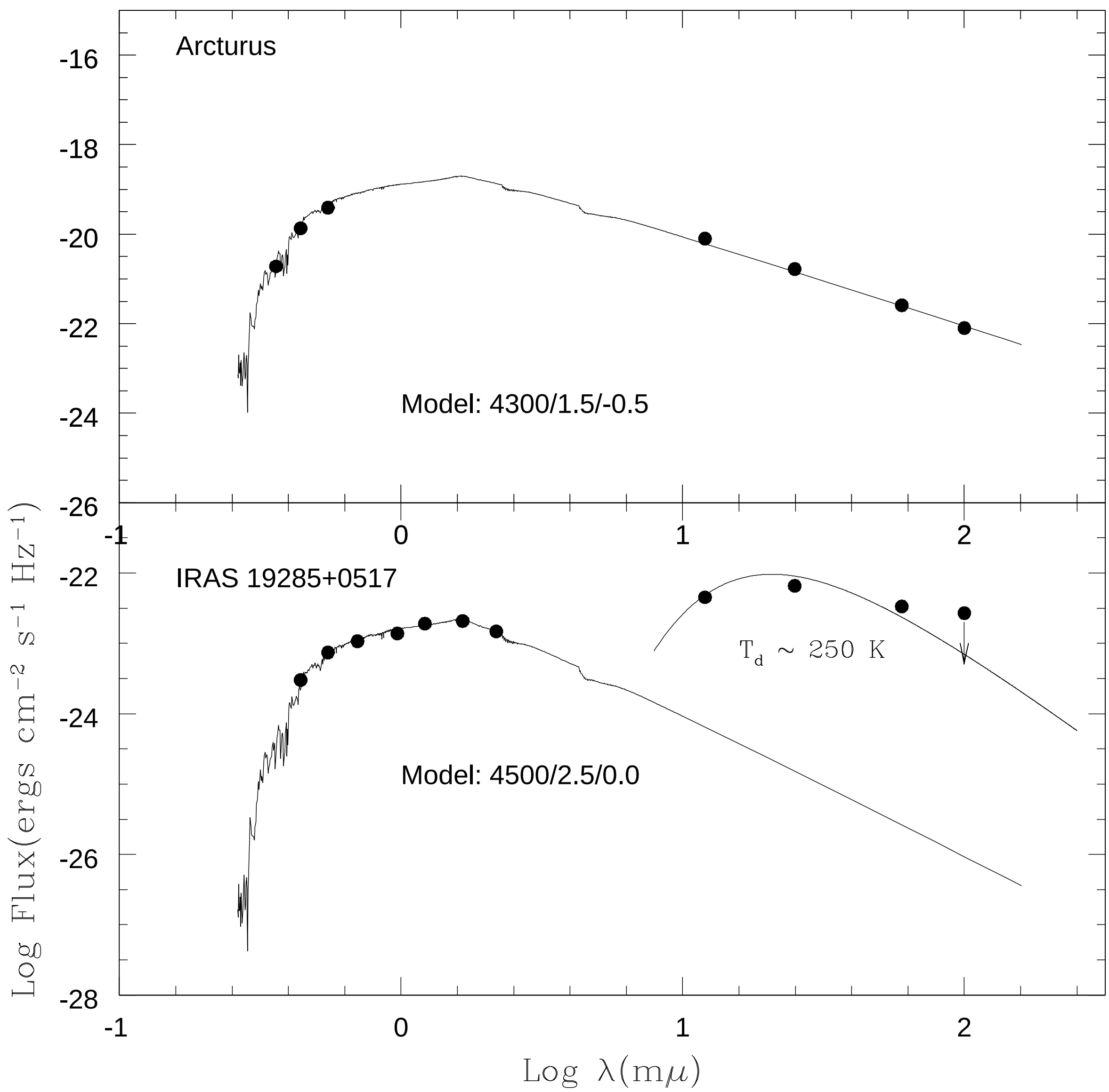
Arcturus
Model: 4300/1.5/-0.5
IRAS 19285+0517
$T_d \sim 250$ K
Model: 4500/2.5/0.0
Log Flux(ergs cm^{-2} s^{-1} Hz^{-1})
Log λ(mμ)
-16
-18
-20
-22
-24
-26
-28
-1
0
1
2

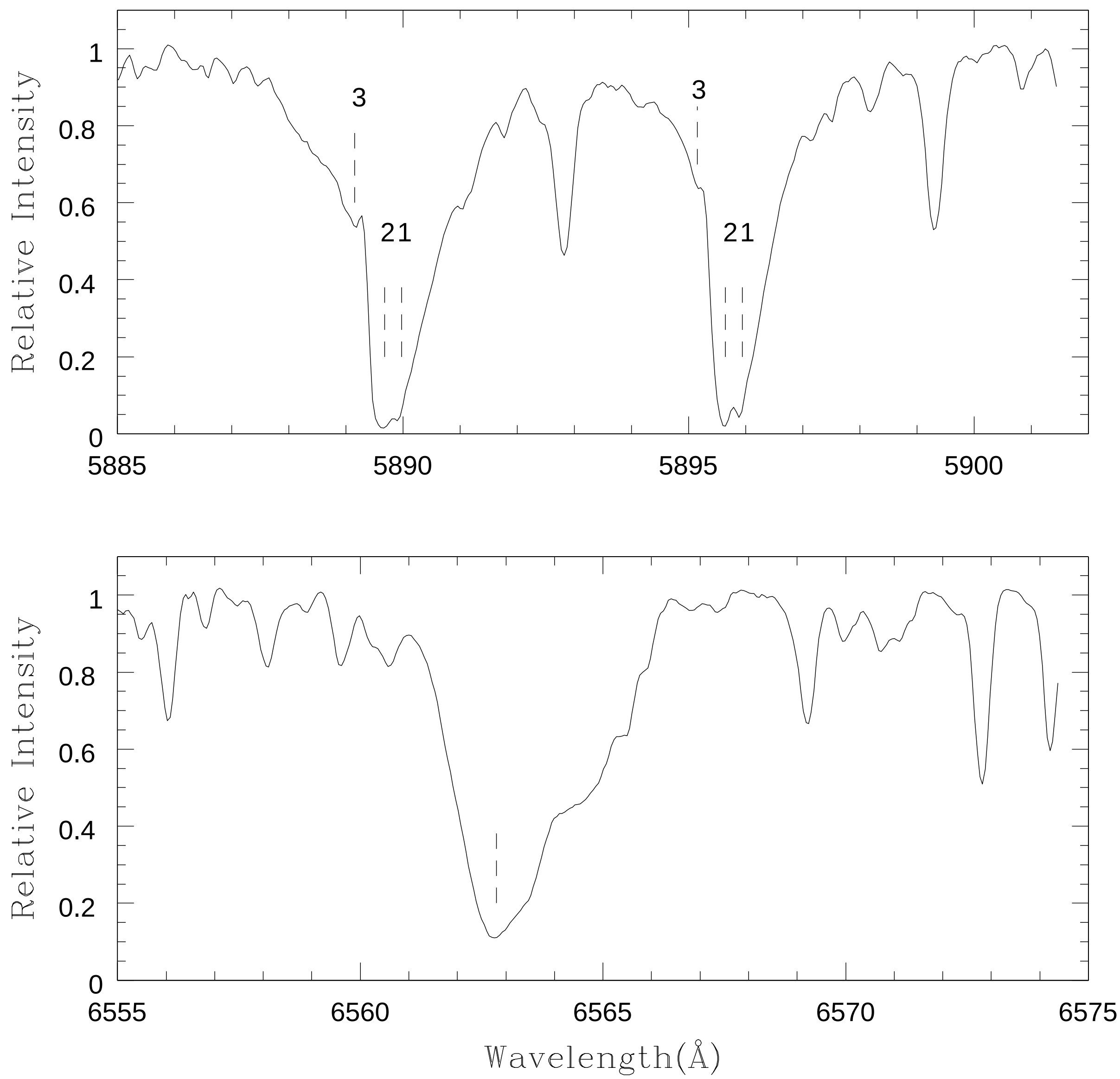

3
21
3
21
Relative Intensity
0
0.2
0.4
0.6
0.8
1
5885
5890
5895
5900
Relative Intensity
0
0.2
0.4
0.6
0.8
1
6555
6560
6565
6570
6575
Wavelength(Å)

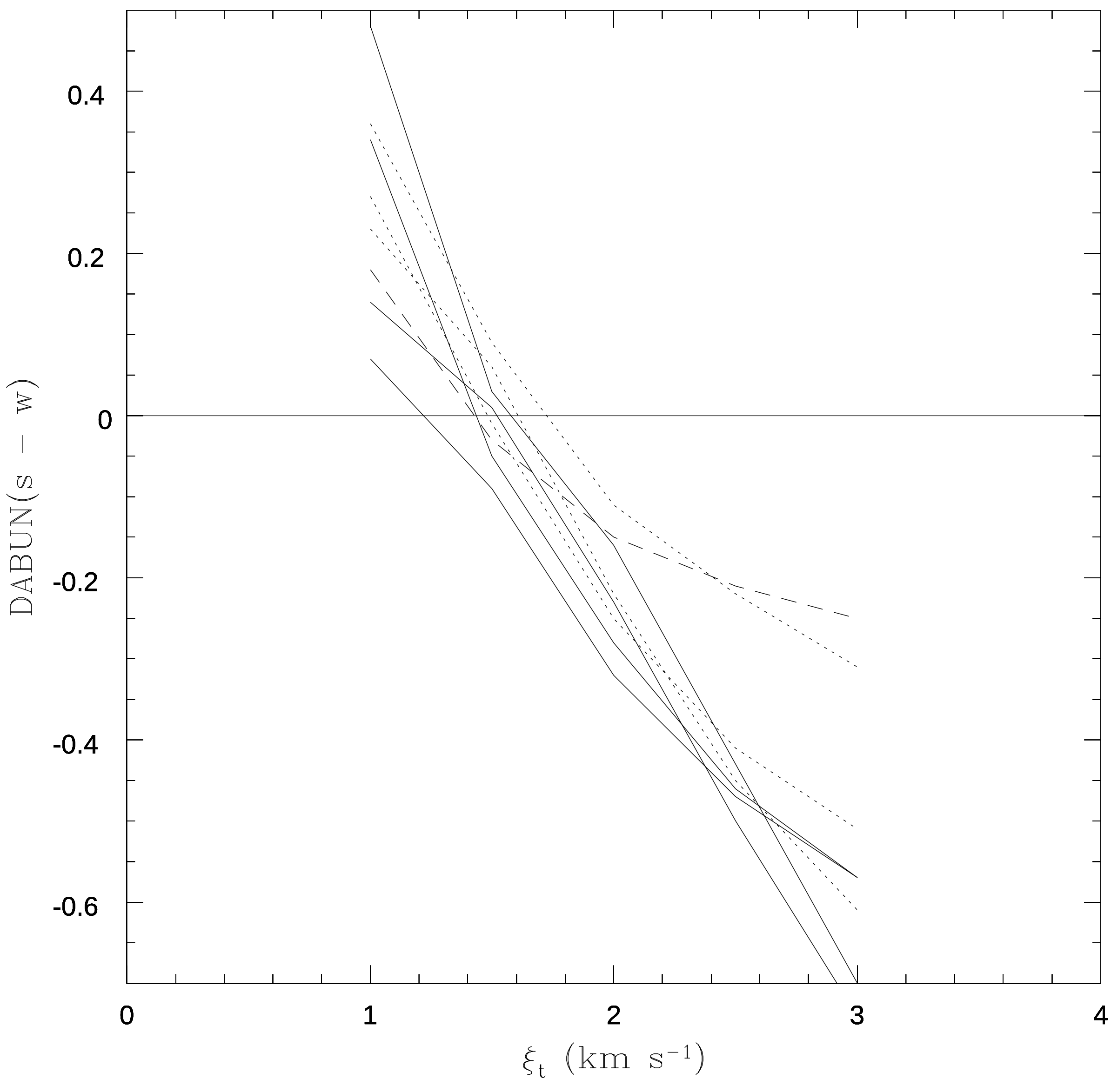
DABUN(s − w)
0.4
0.2
0
-0.2
-0.4
-0.6
0
1
2
3
4
ξt (km s-1)

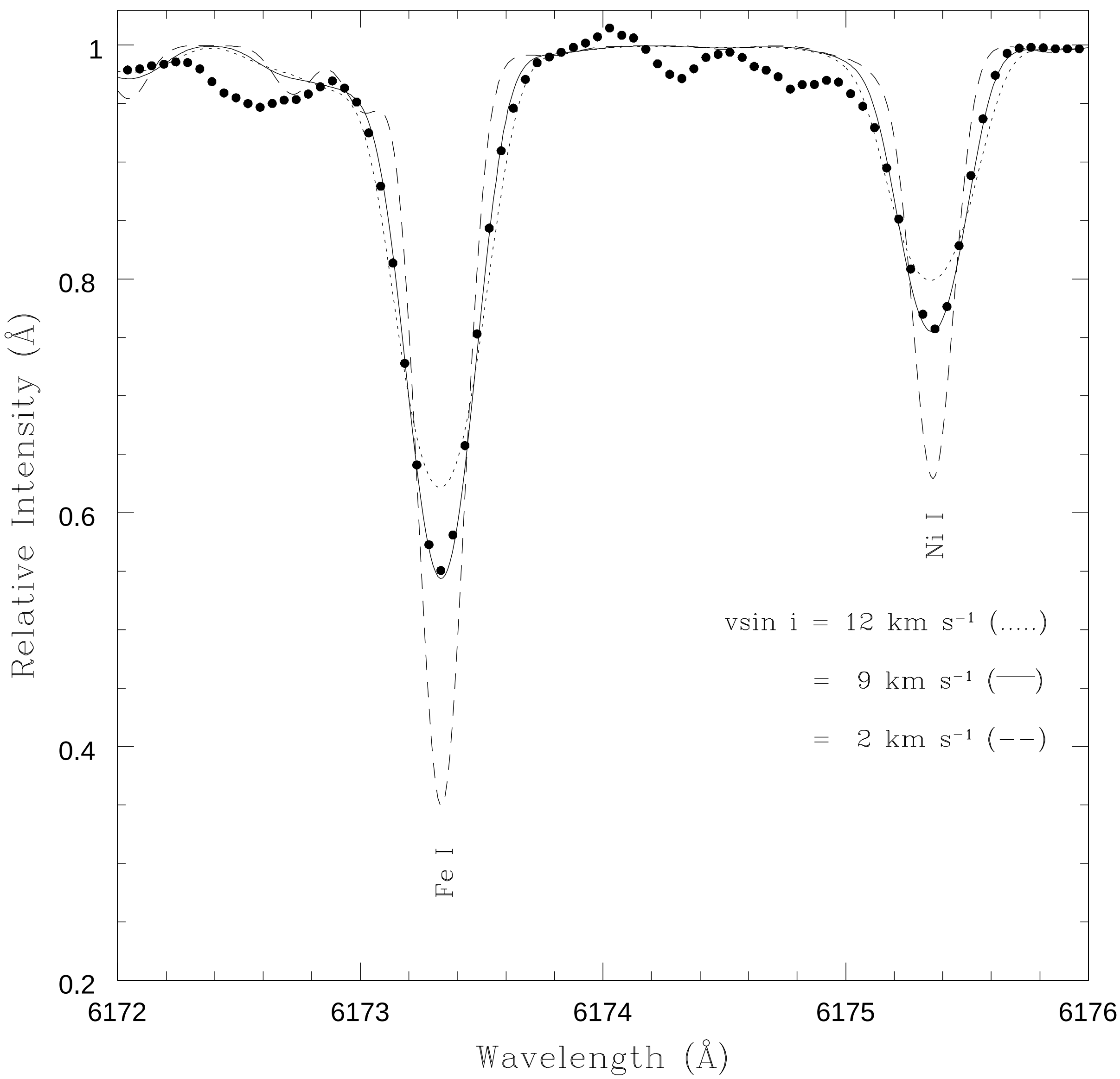
Relative Intensity (Å)
Wavelength (Å)
1
0.8
0.6
0.4
0.2
6172
6173
6174
6175
6176
Fe I
Ni I
vsin i = 12 km s⁻¹ (.....)
= 9 km s⁻¹ (——)
= 2 km s⁻¹ (– –)

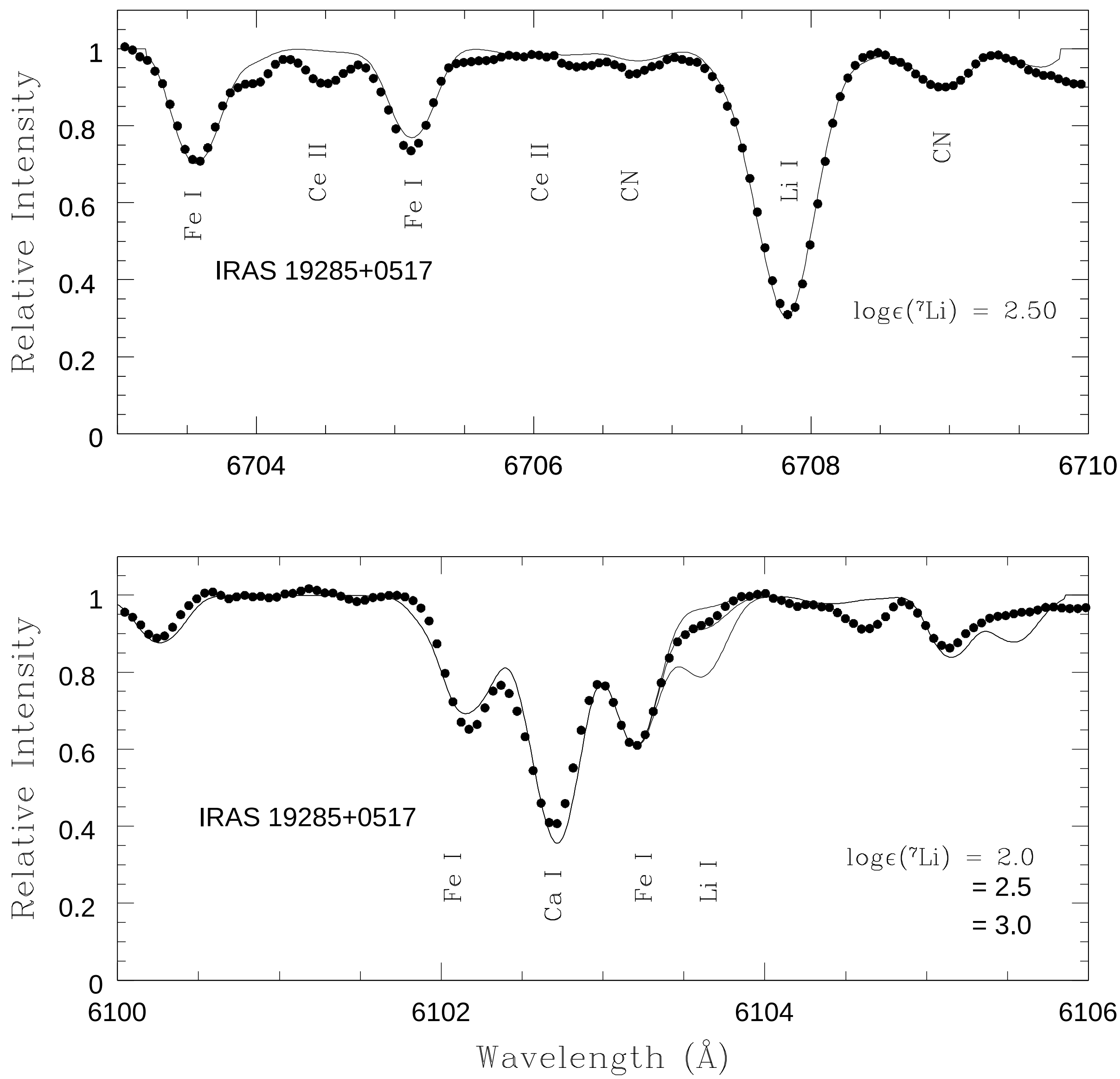

Relative Intensity
Fe I
Ce II
Fe I
Ce II
CN
Li I
CN
IRAS 19285+0517
$\log\epsilon(^7Li)$ = 2.50
6704
6706
6708
6710
Fe I
Ca I
Fe I
Li I
IRAS 19285+0517
$\log\epsilon(^7Li)$ = 2.0
= 2.5
= 3.0
6100
6102
6104
6106
Wavelength (Å)

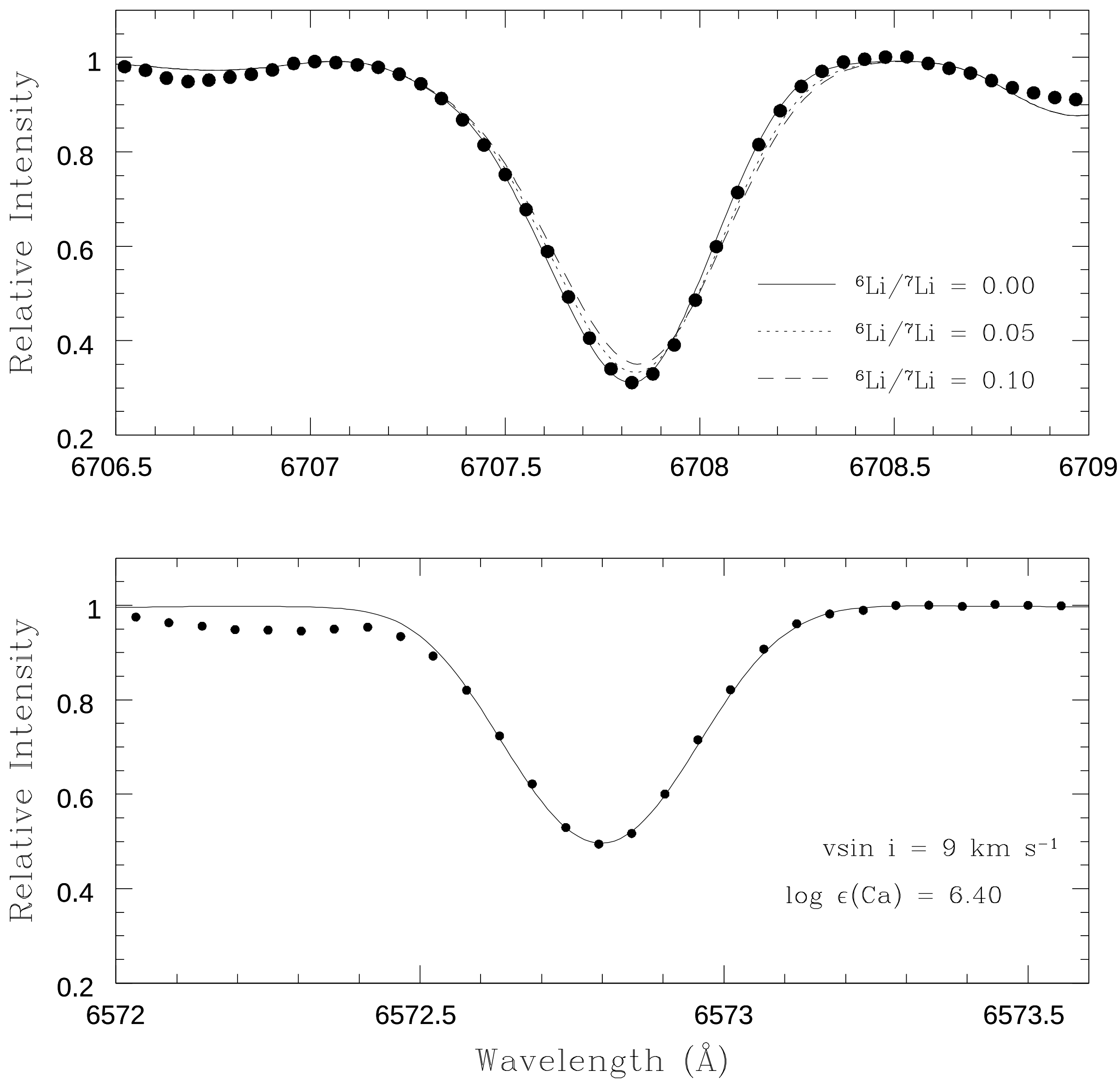
Relative Intensity
1
0.8
0.6
0.4
0.2
6706.5
6707
6707.5
6708
6708.5
6709
⁶Li/⁷Li = 0.00
⁶Li/⁷Li = 0.05
⁶Li/⁷Li = 0.10
Relative Intensity
1
0.8
0.6
0.4
0.2
6572
6572.5
6573
6573.5
vsin i = 9 km s⁻¹
log ϵ(Ca) = 6.40
Wavelength (Å)

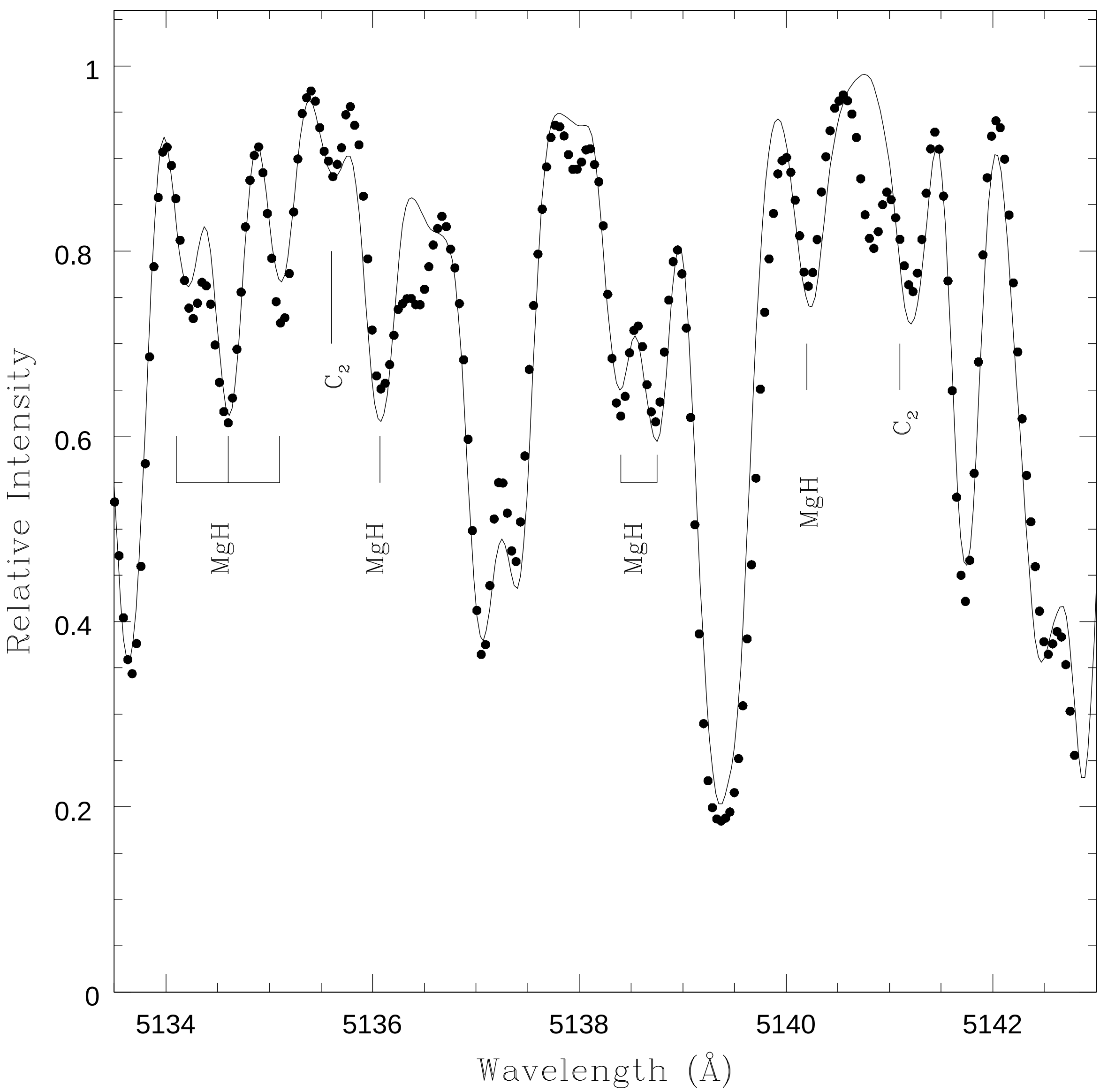
Relative Intensity
Wavelength (Å)
0
0.2
0.4
0.6
0.8
1
5134
5136
5138
5140
5142
MgH
MgH
MgH
MgH
C_2
C_2

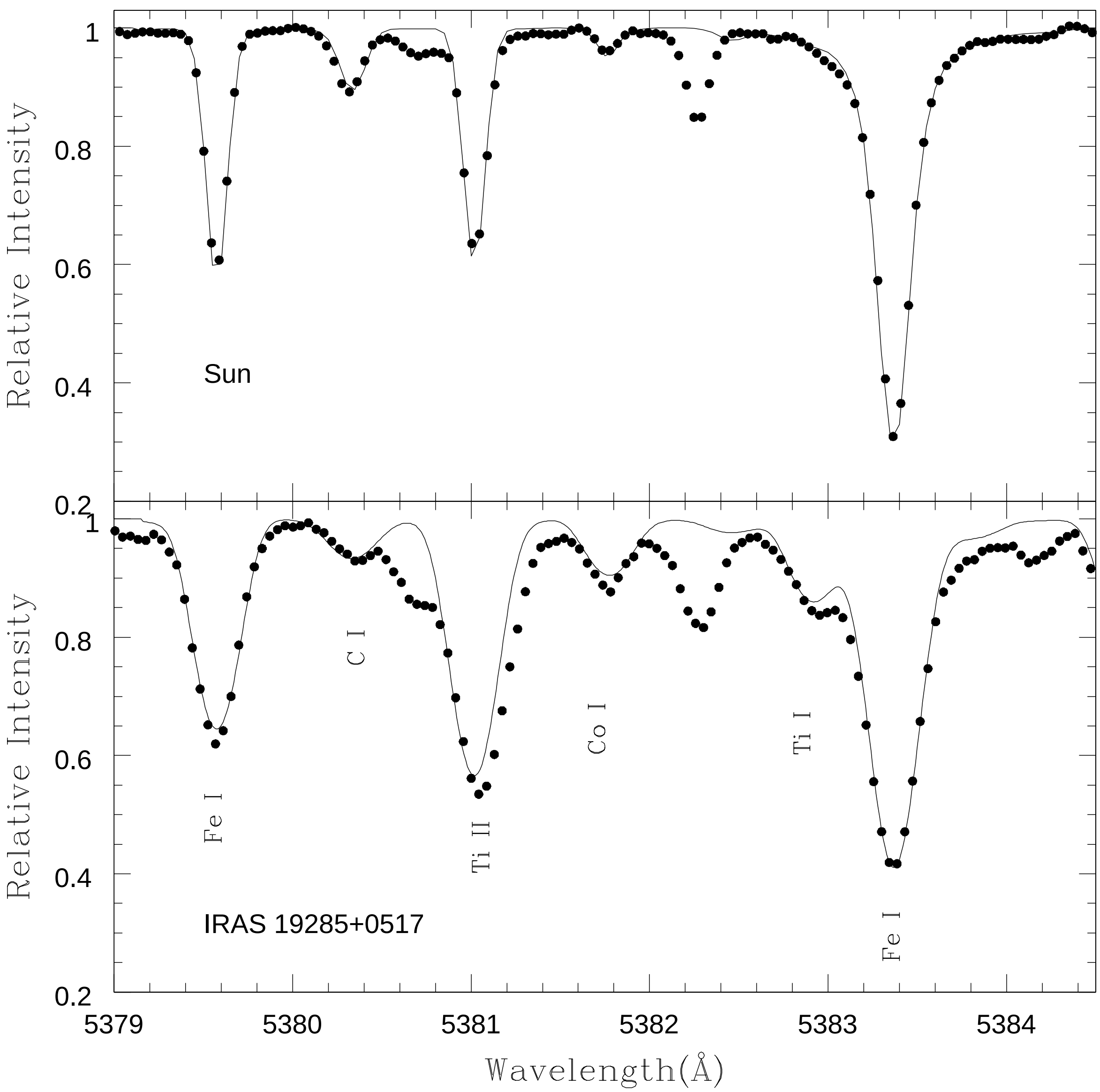
Relative Intensity
Sun
Relative Intensity
IRAS 19285+0517
Fe I
C I
Ti II
Co I
Ti I
Fe I
Wavelength(Å)
1
0.8
0.6
0.4
0.2
5379
5380
5381
5382
5383
5384

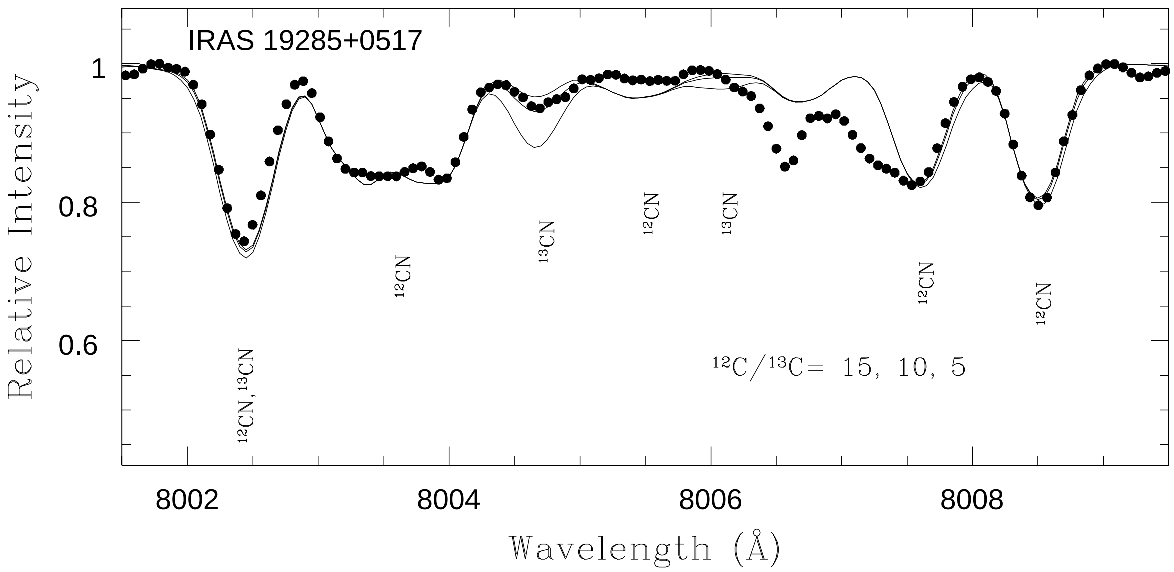

IRAS 19285+0517
Relative Intensity
1
0.8
0.6
^{12}CN,^{13}CN
^{12}CN
^{13}CN
^{12}CN
^{13}CN
^{12}CN
^{12}CN
^{12}C/^{13}C= 15, 10, 5
8002
8004
8006
8008
Wavelength (Å)